CHAPTER IV
RESULTS AND DISCUSSION

4.1 Commercial Plaster of Paris

4.1.1 Pellet Surface Characteristics

Commercial plaster surfaces were observed at various flow rates from 40 to 199 ml/min for three minutes. The dissolution areas of pellets are likely within the circles shown in the SEM pictures (e.g., Figure 4.1), which contain craters from the driving force of the impinging jet. From Figure 4.1 at 199 ml/min, inside of the deeper craters cannot be seen.

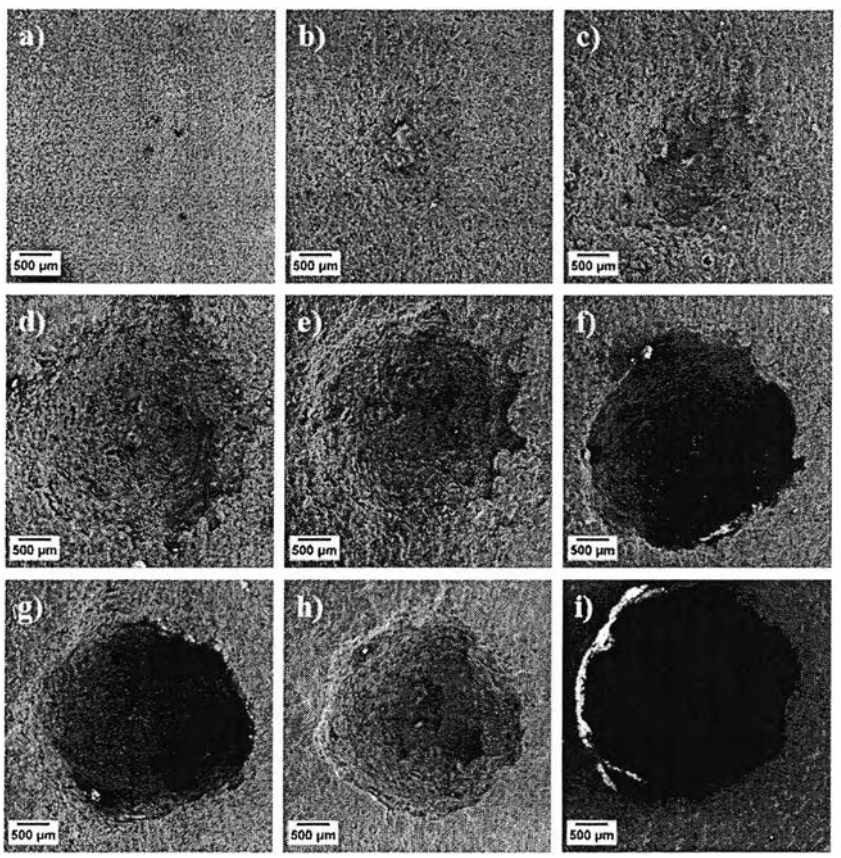

Figure 4.1 Surface of commercial plaster of Paris pellet at different flow rates at 25°C for 3 minutes (a) Before the experiment b) 40 ml/min c) 60 ml/min d) 80 ml/min e) 100 ml/min f) 120 ml/min g) 140 ml/min h) 160 ml/min i) 199 ml/min).

Figure 4.2 shows the surface roughness similar to scallops inside the crater of the pellets. At the lower flow rates, the pellet seems more porous. However, size and population of pores were not uniform.

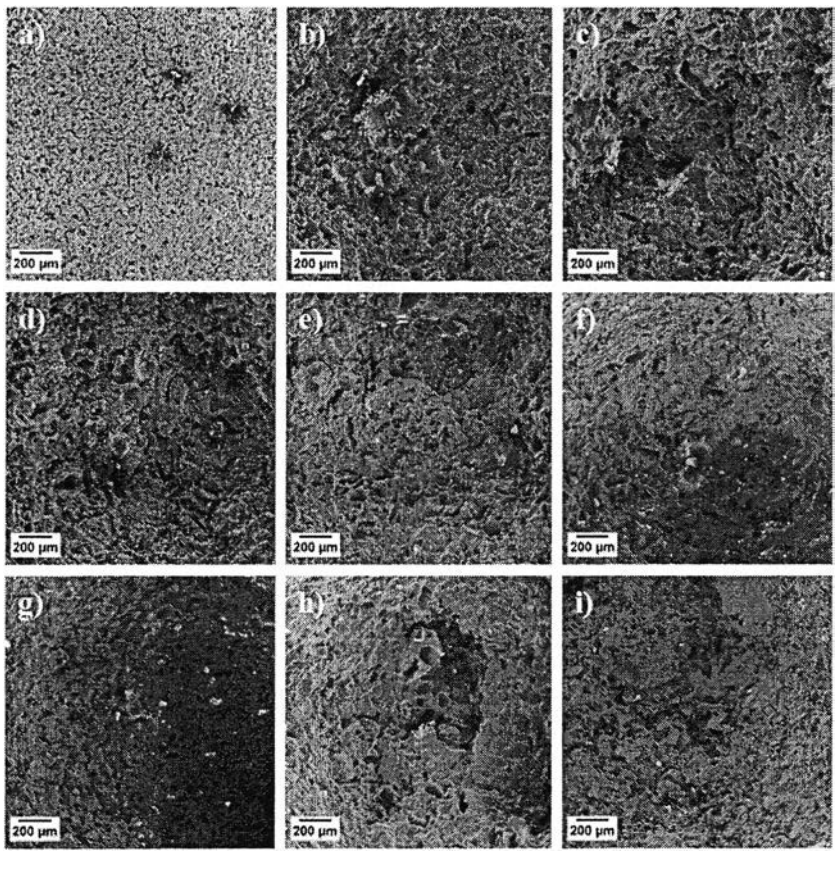

Figure 4.2 Surface of commercial plaster of Paris pellet at different flow rates at 25°C for 3 minutes (a) Before the experiment b) 40 ml/min c) 60 ml/min d) 80 ml/min e) 100 ml/min f) 120 ml/min g) 140 ml/min h) 160 ml/min i) 199 ml/min).

From Figure 4.3 at high magnification, the structure of commercial plaster looks like needles that link together. The needles inside the pellets were found to be more separated as the flow rates increased. These results suggest that commercial plaster released particles (needles) at the higher flows.

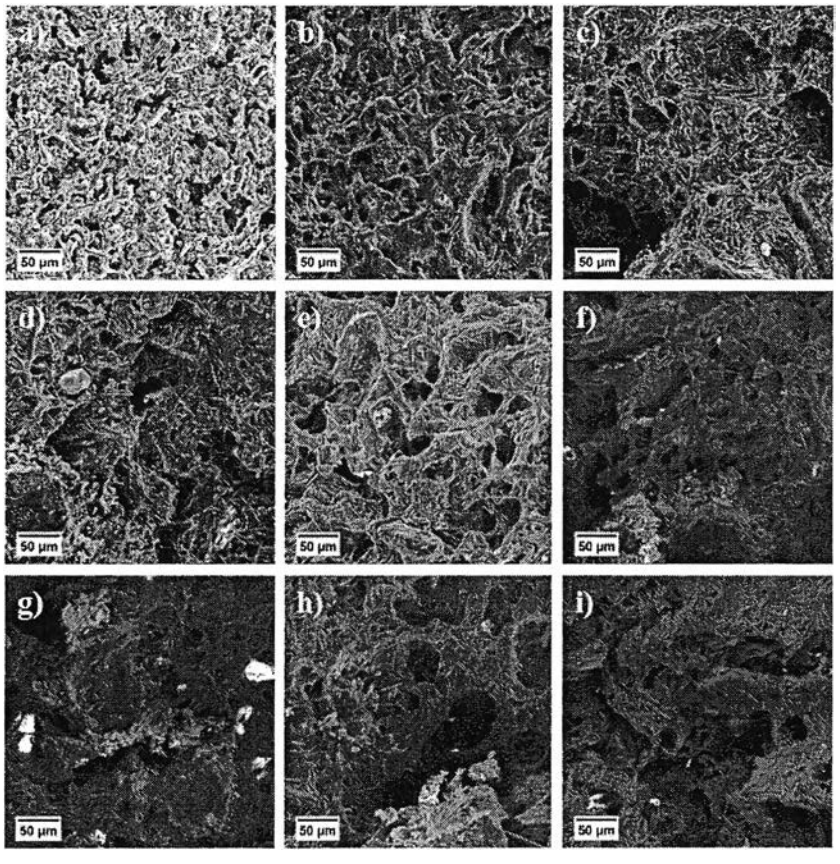

Figure 4.3 Surface of commercial plaster of Paris pellet at different flow rates at 25°C for 3 minutes (a) Before the experiment b) 40 ml/min c) 60 ml/min d) 80 ml/min e) 100 ml/min f) 120 ml/min g) 140 ml/min h) 160 ml/min i) 199 ml/min).

The size of the scallops was not uniform; the different flow rates caused different scallops, as seen in Figure 4.2 and Figure 4.3. The defect theory affirms that the position of each erosional mark is due to the initial presence of an irregularity or a defect at the surface. One can conclude that the characteristics of any assemblage of erosional marks depend on the duration of the eroding process, the spatial distribution, shape and dimensions of the defects and the character of the flow.

4.1.2 Weight Loss

The weight loss of commercial plaster is determined from the volume loss and density of material, because the measurement from weight loss tends to be

inaccurate because of inadvertent loss of material from the bulk of the pellet during handling. Figure 4.4 and Table 4.1 show the increasing amount of material lost with increasing flow rate. The relationship is almost linear at low flows, then tends to level off - but not to a plateau.

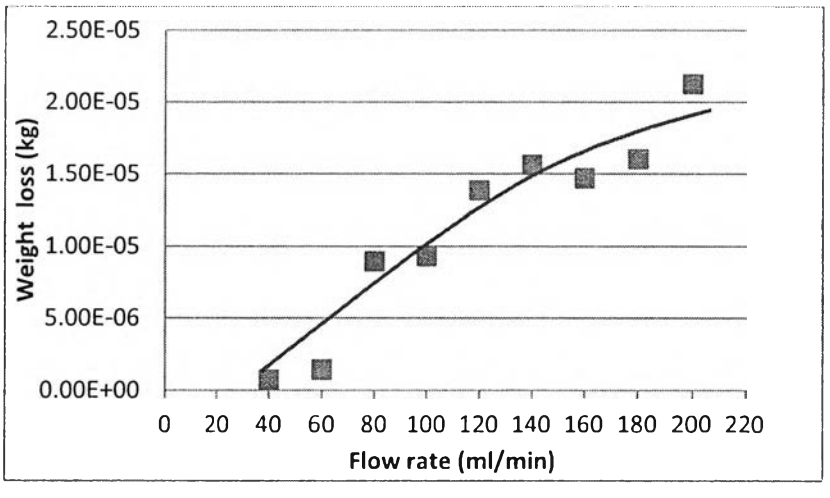

Figure 4.4 The effect of flow rate on weight loss of commercial plaster of Paris pellet.

Table 4.1 The effect of flow rate on volume lost and weight loss in commercial plaster of Paris

Flow rate ml/min	Volume m^3	Weight loss kg
199	2.01E-08	2.13E-05
180	1.52E-08	1.61E-05
160	1.39E-08	1.47E-05
140	1.48E-08	1.56E-05
120	1.31E-08	1.39E-05
100	8.82E-09	9.32E-06
80	8.48E-09	8.95E-06
60	1.37E-09	1.44E-06
40	6.91E-10	7.30E-07

4.1.3 Dissolution Rate

At higher flow rate the dissolution rate was higher than at lower flow rate and appeared to reach a plateau (Figure 4.5). Below 100 - 120 ml/min, the dissolution rate increased linearly with increasing fluid velocity, apparently controlled by mass transfer. Thus, from the studies of Liu and Nacollas (1971), James and Lupton (1978) and Opdyke et al. (1987), the higher dissolution rate results from a thinner boundary layer. Increasing the fluid velocity will decrease the thickness of the boundary layer and make the concentration gradient in the boundary layer steeper. In addition, the formation of scallops causes the surface area of plaster to increase, which also causes a higher dissolution rate. These results confirm the study of Villien et al. (2005); when the diffusion transfer is relatively low and/or the dissolution rate at the surface is high, molecular diffusion is the limiting step. The dissolution rate departs from the linear relation with flow at 120 to 199 ml/min. According to the study of Villien et al. (2005), when the diffusion transfer is high enough to ensure that the surface concentration of the dissolved species is close to that in the bulk flow, the rate of dissolution is controlled by the reaction rate at the

surface. The trend line seems to confirm the study of Villien et al. The leveling off of the dissolution rate to a plateau above flow rate of 120 ml/min suggests a limiting mass transfer rate and dissolution control of 3.25E-03 kg/m^2·s. However, it is possible that the scatter of the data mask a slightly increasing dissolution rate with flow at the higher flows – perhaps because of the release of particles (needles) as dissolution proceeds.

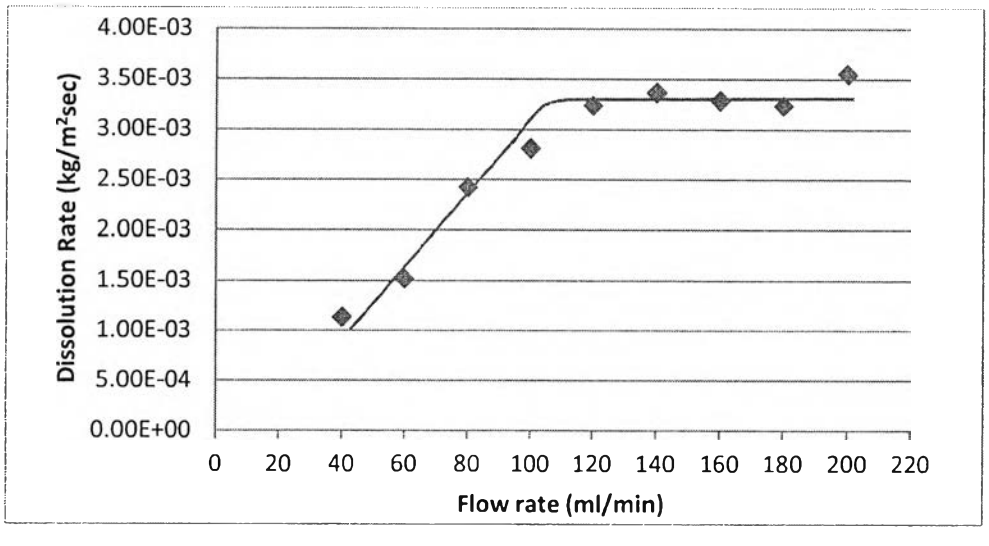

Figure 4.5 Dissolution rate of commercial plaster of Paris with different flow rates.

Table 4.2 Dissolution rate of commercial plaster of Paris with different flow rates

Flow rate ml/min	Dissolution Rate $kg/m^2 \cdot sec$
199	3.55E-03
180	3.24E-03
160	3.29E-03
140	3.37E-03
120	3.24E-03
100	2.81E-03
80	2.42E-03
60	1.52E-03
40	1.13E-03

4.1.4 Overall Rate Constant

Figure 4.6 and Table 4.3 show the overall rate constants, which are increased by increasing the fluid flow rate. The constants from the overall rates (K) show the same trend as the dissolution rates. They are derived from the expression Dissolution rate = $K(C_s-C_b)$ where C_s = solubility and C_b = bulk concentration (zero in this experiment). Since, assuming a plateau for the data at high flow, there was dissolution control at above 120 ml/min, the dissolution rate constant of commercial plaster can be determined as 1.58E-03 m/s.

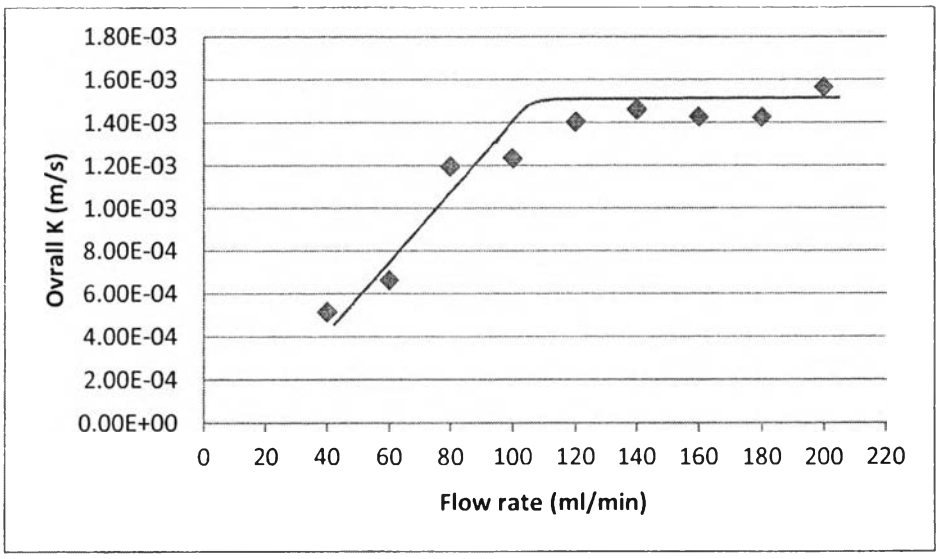

Figure 4.6 Overall rate constant of commercial plaster of Paris with different flow rates.

Table 4.3 Overall rate constant of commercial plaster of Paris with different flow rates

Flow rate ml/min	Overall K m/s
199	1.73E-03
180	1.58E-03
160	1.60E-03
140	1.64E-03
120	1.58E-03
100	1.37E-03
80	1.18E-03
60	7.40E-04
40	5.52E-04

4.2 Pure Plaster of Paris

4.2.1 Pellet Surface Characteristics

Pure plaster experiments were performed at 35°C for 5 minutes at flow rates ranging from 40 to 180 ml/min. The dissolution areas of pellets are not uniform like commercial plaster. The driving force of impinging jet obviously creates an irregular spread mark at low flow rate. However, the dissolution areas at high flow rate (160 ml/min and 180 ml/min) are more likely the circle area.

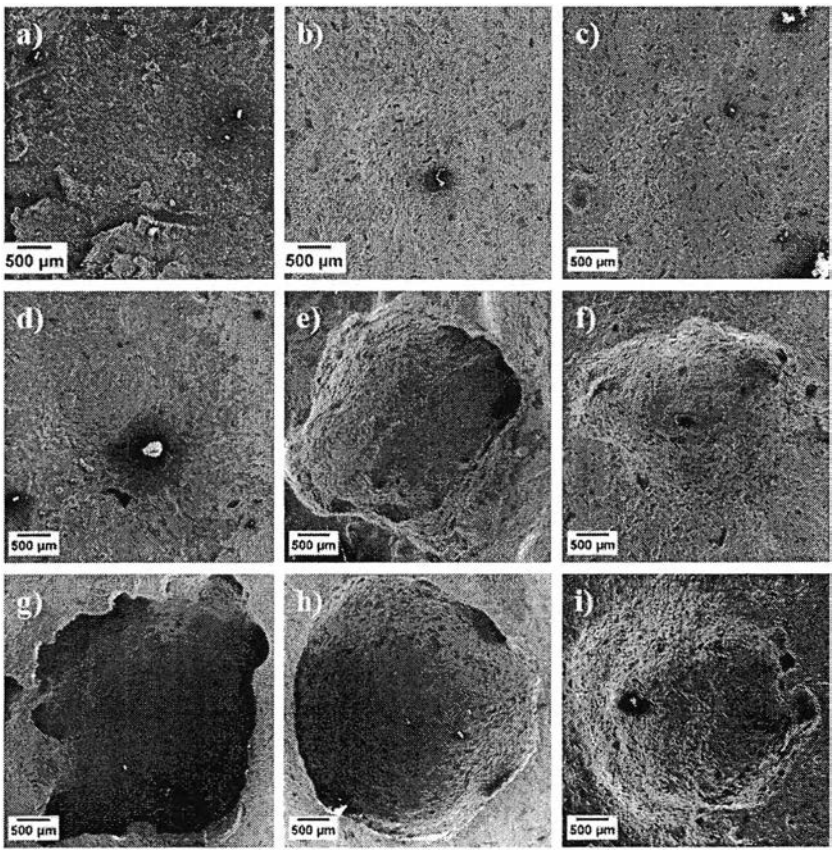

Figure 4.7 Surface of pure plaster of Paris pellet at different flow rates at 35°C for 10 minutes (a) Before the experiment b) 40 ml/min c) 60 ml/min d) 80 ml/min e) 100 ml/min f) 120 ml/min g) 140 ml/min h) 160 ml/min i) 180 ml/min).

The surfaces inside the pellet craters (Figure 4.8) show that porosity of the pure plaster increases when the flow rate increases. From Figure 4.9, the structure of pure plaster looks similar to that of the commercial plaster, but the needles of pure plaster are smaller and more densely packed than those of pure plaster. It suggests that the pure plaster is less likely than commercial plaster to release particles.

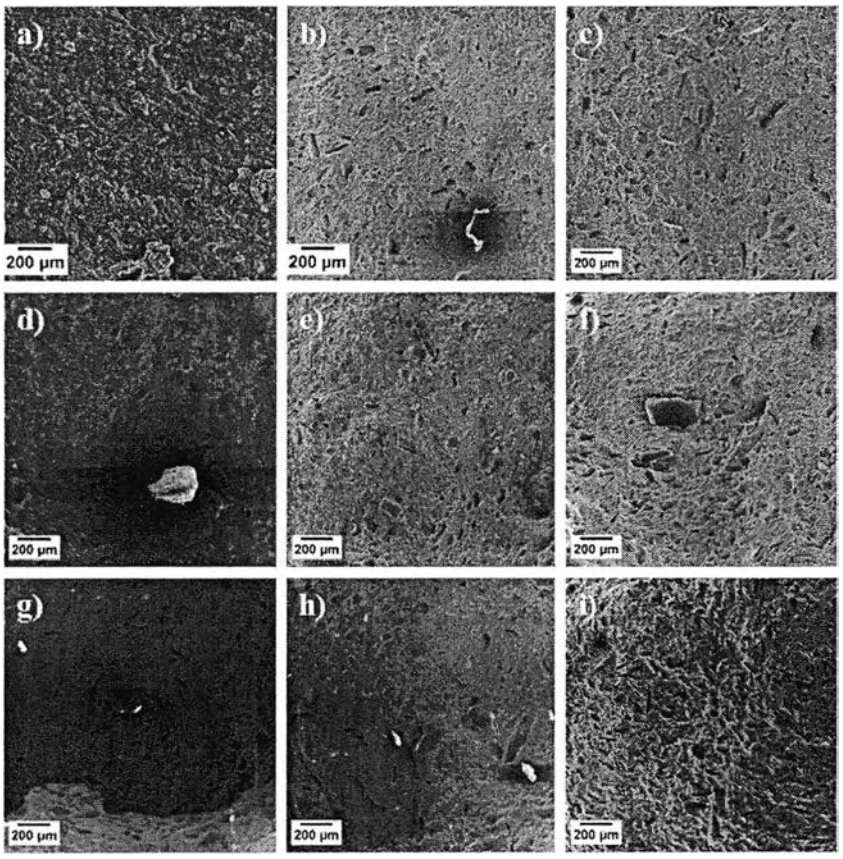

Figure 4.8 Surface of pure of Paris pellet at different flow rates at 35°C for 10 minutes (a) Before the experiment b) 40 ml/min c) 60 ml/min d) 80 ml/min e) 100 ml/min f) 120 ml/min g) 140 ml/min h) 160 ml/min i) 180 ml/min).

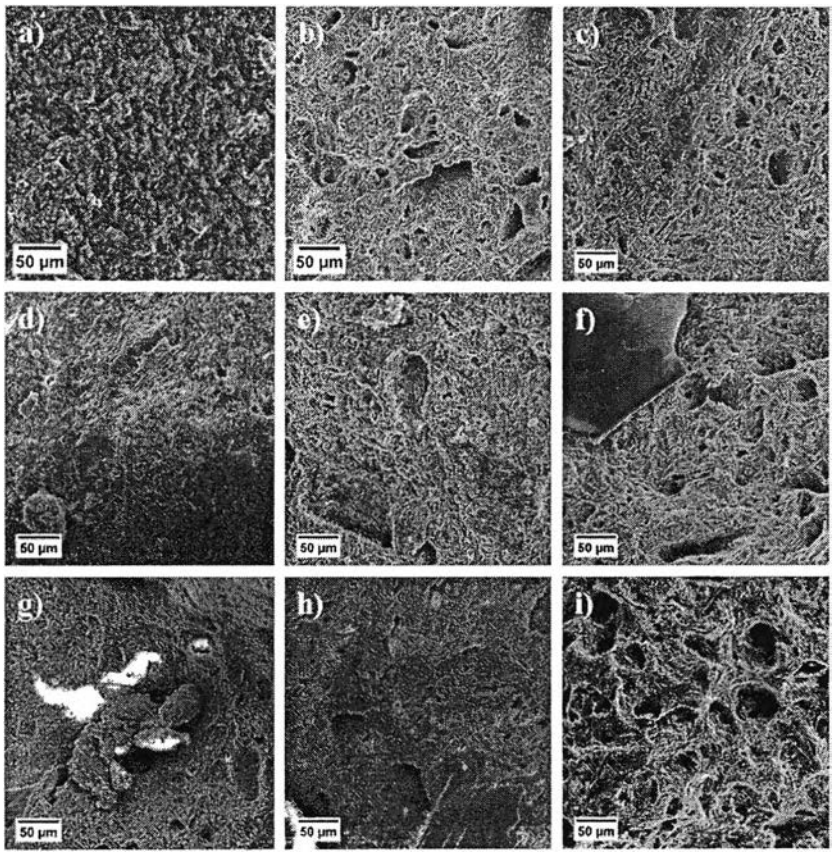

Figure 4.9 Surface of pure of Paris pellet at different flow rates at 35°C for 10 minutes (a) Before the experiment b) 40 ml/min c) 60 ml/min d) 80 ml/min e) 100 ml/min f) 120 ml/min g) 140 ml/min h) 160 ml/min i) 180 ml/min).

4.2.2 Weight Loss

The weight loss of pure plaster increases significantly with increasing fluid flow rate, although the scatter in the data is quite high. Note that the overall weight loss of pure plaster is greater than that of the commercial plaster – probably because the pure plaster experiments were carried at higher temperature (34°C).

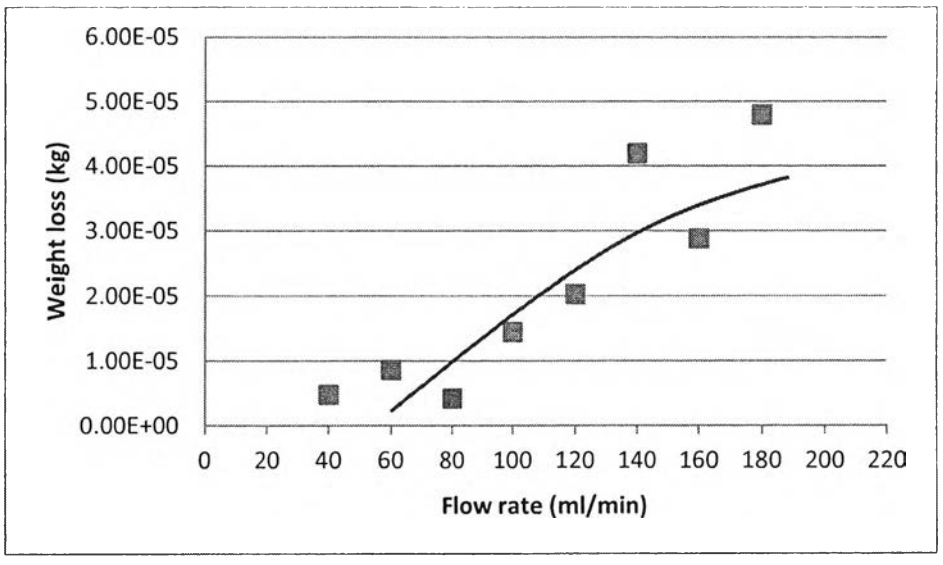

Figure 4.10 The effect of flow rate on weight loss of pure plaster of Paris pellet.

Table 4.4 The effect of flow rate on volume lost and weight loss in pure plaster of Paris

Flow rate ml/min	Volume m^3	Weight loss kg
180	4.03E-08	4.80E-05
160	2.42E-08	2.88E-05
140	3.52E-08	4.20E-05
120	1.70E-08	2.03E-05
100	1.21E-08	1.45E-05
80	3.56E-09	4.24E-06
60	7.25E-09	8.63E-06
40	4.05E-09	4.82E-06

4.2.3 Dissolution Rate

The leveling-off the pure plaster dissolution with flow is less obvious than that of the commercial plaster – possible because of the higher scatter of the data. Liu and Nacollas (1971) studied the dissolution rate constant of plaster of Paris

at 10° and 30°C with the Arrhenius equation. They found that the activation energy was greater than expected on the basis of pure mass-transport control. According to most of studies, diffusion across the liquid boundary layer is the rate-controlling step, but it is not possible in the light of this relatively large activation energy. This may suggest a more complicated mechanism. The pure plaster dissolution is possibly under mixed transport/reaction control, where the transport-controlled kinetics dominate the initial dissolution and the surface reaction kinetics become more important later, which is in agreement with Raines and Dewers, (1997).

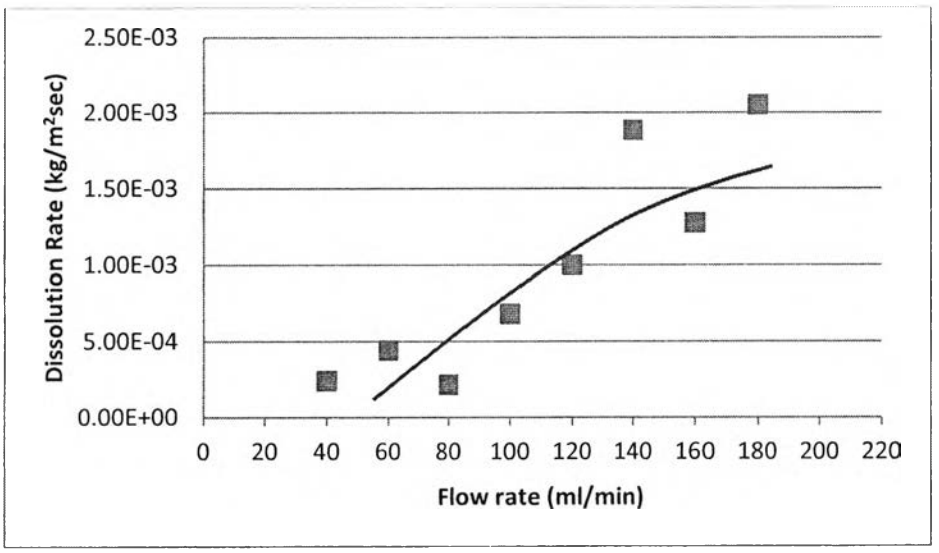

Figure 4.11 Dissolution rate of pure plaster of Paris with different flow rates.

Table 4.5 Dissolution rate of pure plaster of Paris at different flow rates

Flow rate ml/min	Dissolution Rate $kg/m^2 \times sec$
180	2.05E-03
160	1.27E-03
140	1.89E-03
120	9.98E-04
100	6.81E-04
80	2.16E-04
60	4.43E-04
40	2.41E-04

4.2.4 Overall Rate Constant

The overall rate constant of pure plaster is shown in Figure 4.12 and Table 4.6. The trend reflects the dissolution rate – as expected. The overall dissolution values for pure plaster are lower than those for commercial plaster, which means that the purity of plaster affects the dissolution characteristic.

From the observations here it can be concluded that the commercial plaster structure is more porous than that of the pure plaster; it can therefore release more particles and have apparently higher dissolution rates and dissolution coefficient.

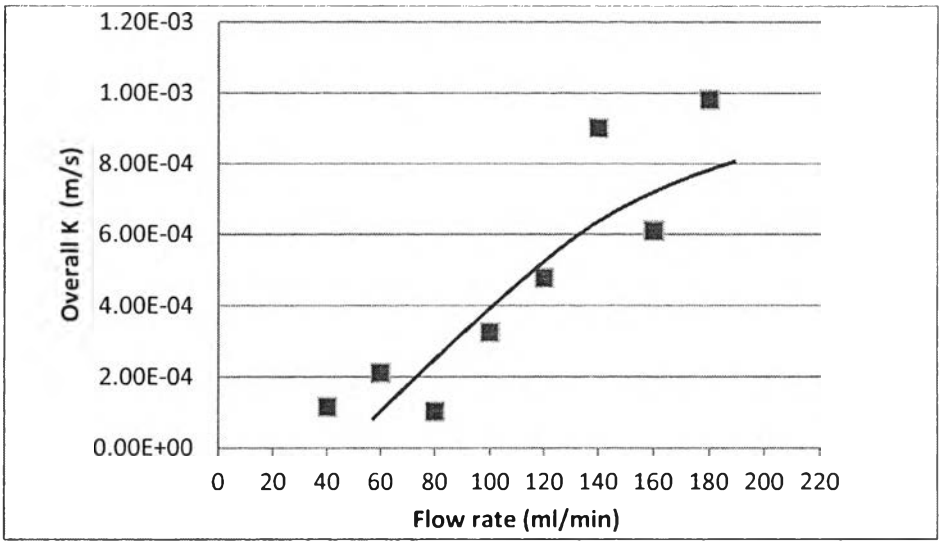

Figure 4.12 Overall rate constant of pure plaster of Paris with different flow rates.

Table 4.6 Overall rate constant of pure plaster of Paris with different flow rates

Flow rate ml/min	Overall K m/s
180	9.82E-04
160	6.10E-04
140	9.02E-04
120	4.78E-04
100	3.26E-04
80	1.04E-04
60	2.12E-04
40	1.16E-04

4.3 Potassium Bitartrate

4.3.1 Pellet Surface Characteristics

The potassium bitartrate pellets were exposed at various flow rates (40 ml/min to 180 ml/min). The potassium bitartrate craters were roughly circular (Figure 4.13). The dissolution area expands with increasing the fluid flow and becomes constant at above 140 ml/min. It means that the jet driving force has less effect with dissolution area at high flow rate.

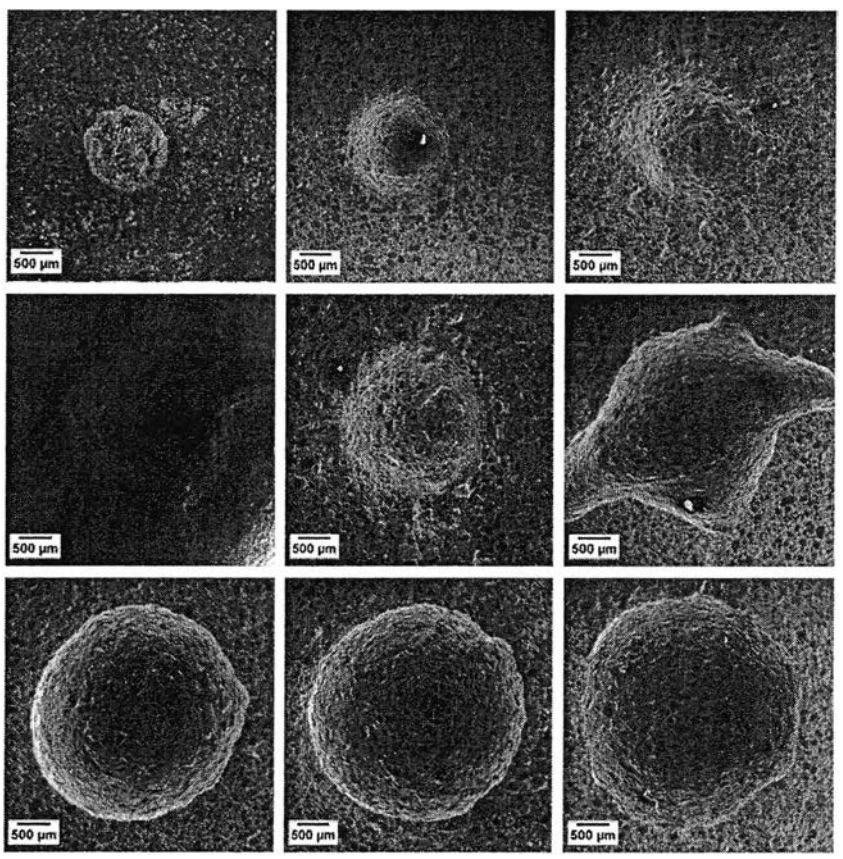

Figure 4.13 Surface of potassium bitartrate pellet at different flow rates at 20°C for 10 minutes (a) Before the experiment b) 40 ml/min c) 60 ml/min d) 80 ml/min e) 100 ml/min f) 120 ml/min g) 140 ml/min h) 160 ml/min i) 180 ml/min).

The surface before the experiment looks different from the surfaces of other materials because of residual potassium bitartrate powder. The surfaces inside the craters are similar comprising well-packed particles.

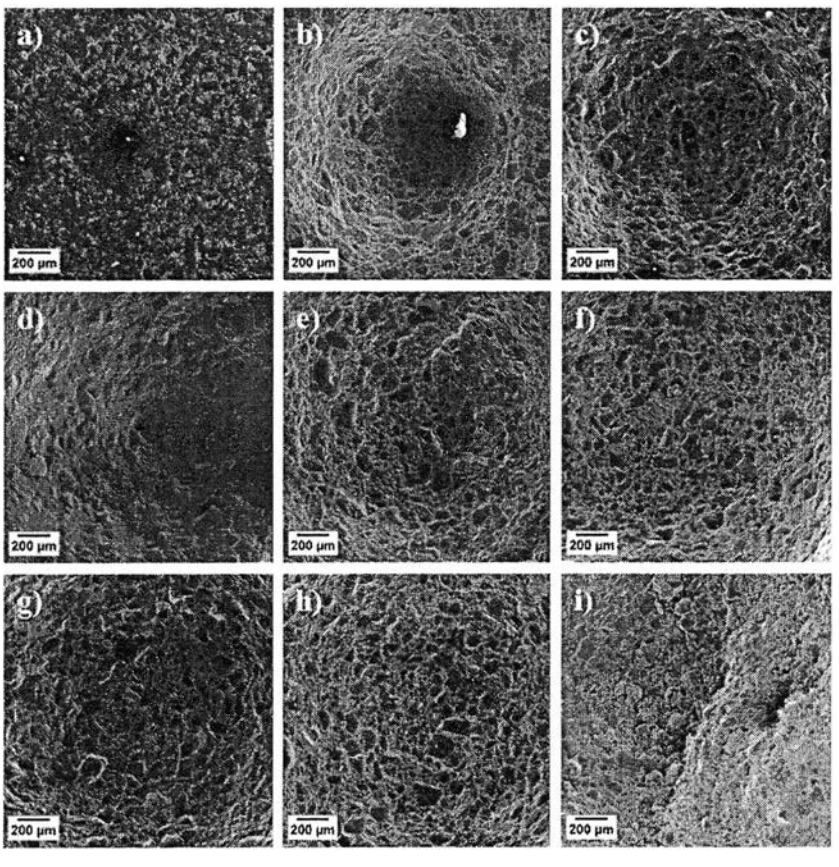

Figure 4.14 Surface of potassium bitartrate pellet at different flow rates at 20°C for 10 minutes (a) Before the experiment b) 40 ml/min c) 60 ml/min d) 80 ml/min e) 100 ml/min f) 120 ml/min g) 140 ml/min h) 160 ml/min i) 180 ml/min).

A small hole appears inside the crater at 80 ml/min, possibly from the release of a big particle at the center of the pellet. In Figure 4.15, there are some small particles on the pellet surface at above 100 ml/min. This suggests that the potassium bitartrate pellet started to release particles markedly at 180 ml/min.

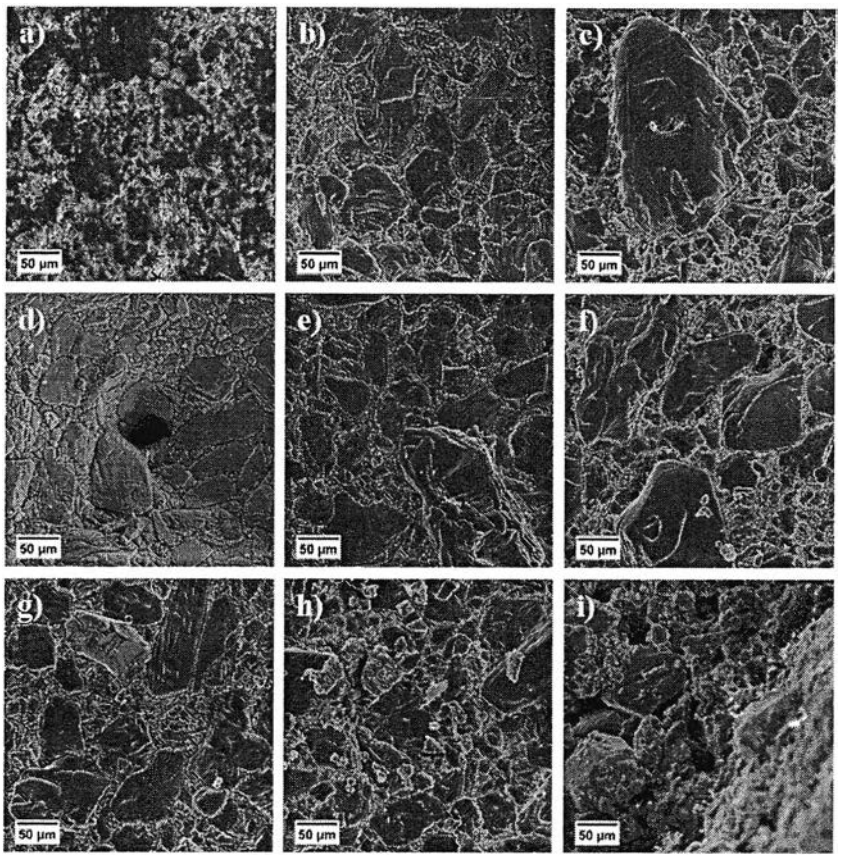

Figure 4.15 Surface of potassium bitartrate pellet at different flow rates at 20°C for 10 minutes (a) Before the experiment b) 40 ml/min c) 60 ml/min d) 80 ml/min e) 100 ml/min f) 120 ml/min g) 140 ml/min h) 160 ml/min i) 180 ml/min).

4.3.2 Weight Loss

The slope of the weight loss data with flow decreases from an approximately linear value at low flow (Figure 4.16 and Table 4.7). The weight loss increases markedly at 180 ml/min, which confirms the hypothesis of releasing particles.

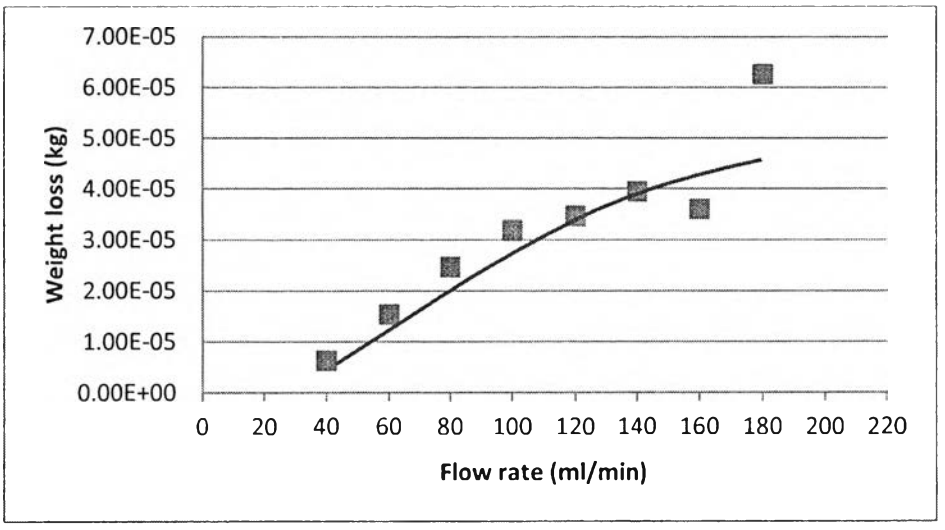

Figure 4.16 The effect of flow rate on weight loss of potassium bitartrate pellet.

Table 4.7 The effect of flow rate on volume lost and weight loss in potassium bitartrate

Flow rate ml/min	Volume m^3	Weight loss kg
180	3.29E-08	6.26E-05
160	1.89E-08	3.60E-05
140	2.07E-08	3.95E-05
120	1.82E-08	3.47E-05
100	1.67E-08	3.19E-05
80	1.30E-08	2.47E-05
60	8.08E-09	1.54E-05
40	3.31E-09	6.30E-06

4.3.3 Dissolution Rate

From Figure 4.17, the dissolution rate of potassium bitartrate increases linearly with flow from 40 ml/min to 100 ml/min. These results can represent mass transfer control. The dissolution rate becomes constant with flow at 100 ml/min to

140 ml/min, and then increases from 160 ml/min to 180 ml/min. However, the trend is likely to be a smooth decrease in rate with flow, masked by the scatter in the data.

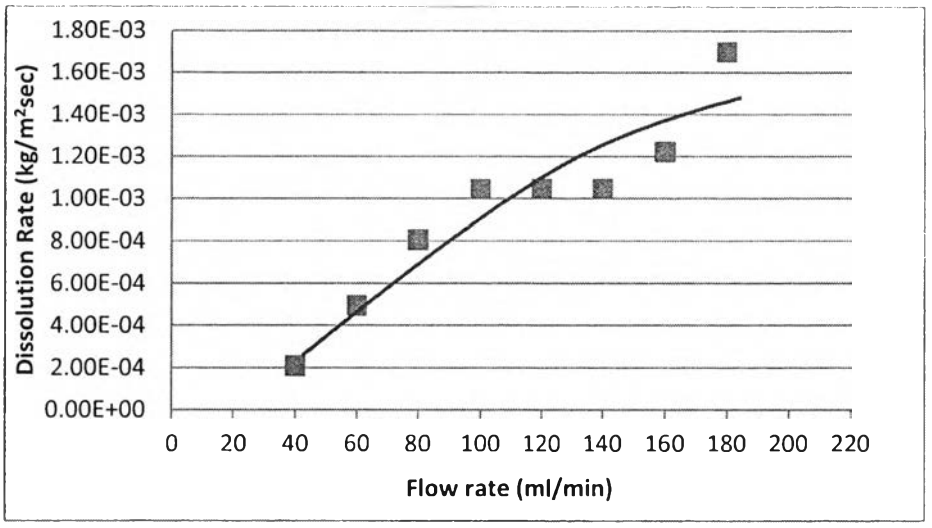

Figure 4.17 Dissolution rate of potassium bitartrate with different flow rates.

Table 4.8 Dissolution rate of potassium bitartrate with different flow rates.

Flow rate ml/min	Dissolution Rate $kg/m^2 \times sec$
180	1.70E-03
160	1.22E-03
140	1.05E-03
120	1.05E-03
100	1.05E-03
80	8.07E-04
60	4.95E-04
40	2.09E-04

4.3.4 Overall Rate Constant

The overall rate constant tends to level off at flows above 100 ml/min (Figure 4.18), no doubt as mass transfer becomes less controlling. The plateau at

100-140 ml/min suggests a rate constant as 1.7E-04 m/s, possibly with particle release increasing at the higher flows. However, the plateau may be an artifact of the data scatter.

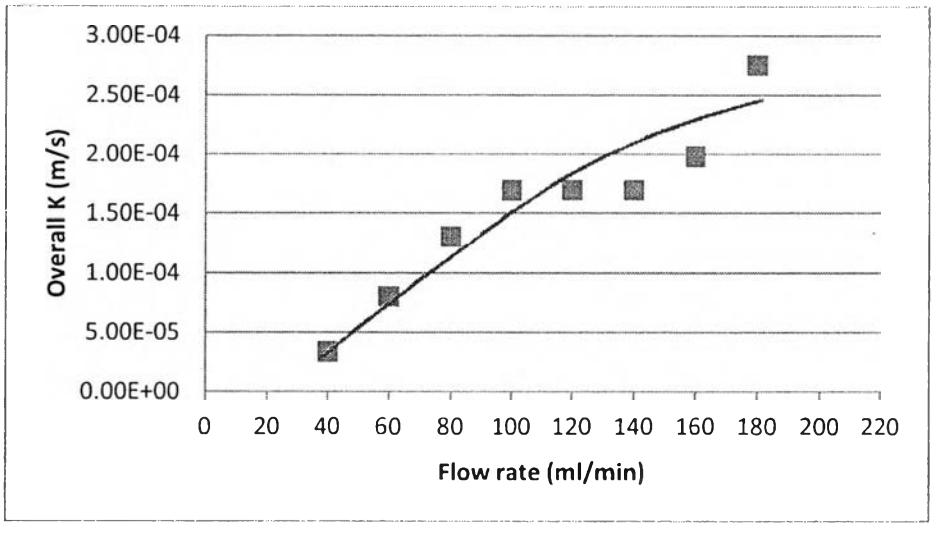

Figure 4.18 Overall rate constant of potassium bitartrate with different flow rates.

Table 4.9 Overall rate constant of potassium bitartrate with different flow rates

Flow rate ml/min	Overall K m/s
180	2.75E-04
160	1.98E-04
140	1.70E-04
120	1.70E-04
100	1.69E-04
80	1.31E-04
60	8.02E-05
40	3.39E-05

4.4 L-Aspartic Acid

4.4.1 Pellet Surface Characteristics

L-aspartic acid is more powdery than the other materials. L-aspartic acid surfaces were observed at various flow rates from 40 to 180 ml/min for 5 minutes. The dissolution areas are not entirely uniform, but the craters are roughly circular. Note that the dissolution area at 100 ml/min is different from those at other flow rates (Figure 4.19); it contains a small but deep crater inside. From Figure 4.20 and 4.21, one can see small particles on the surface of the crater and note that the porosity obviously increases with increasing fluid velocity. These results can be explained by the l-aspartic acid particles being easy to be released. If the particles agglomerate, large ones may release more easily and create deep holes or cracks. This seems to be the explanation for the non-uniform craters at various flow rates.

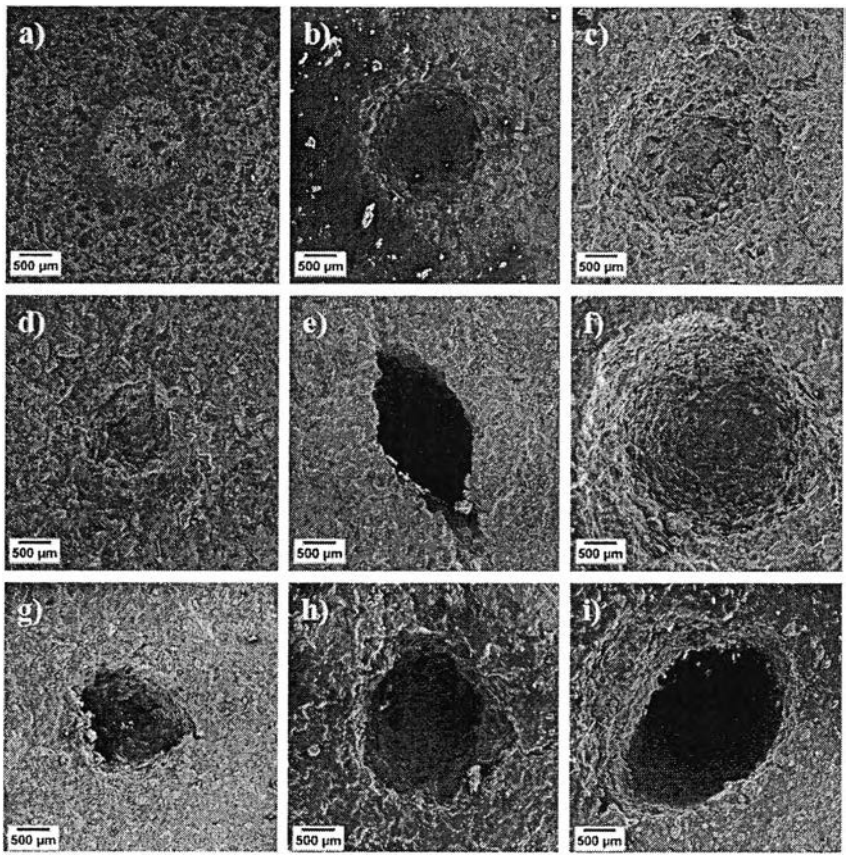

Figure 4.19 Surface of l-aspartic acid pellet at different flow rates at 20 °C for 5 minutes (a) Before the experiment b) 40 ml/min c) 60 ml/min d) 80 ml/min e) 100 ml/min f) 120 ml/min g) 140 ml/min h) 160 ml/min i) 180 ml/min).

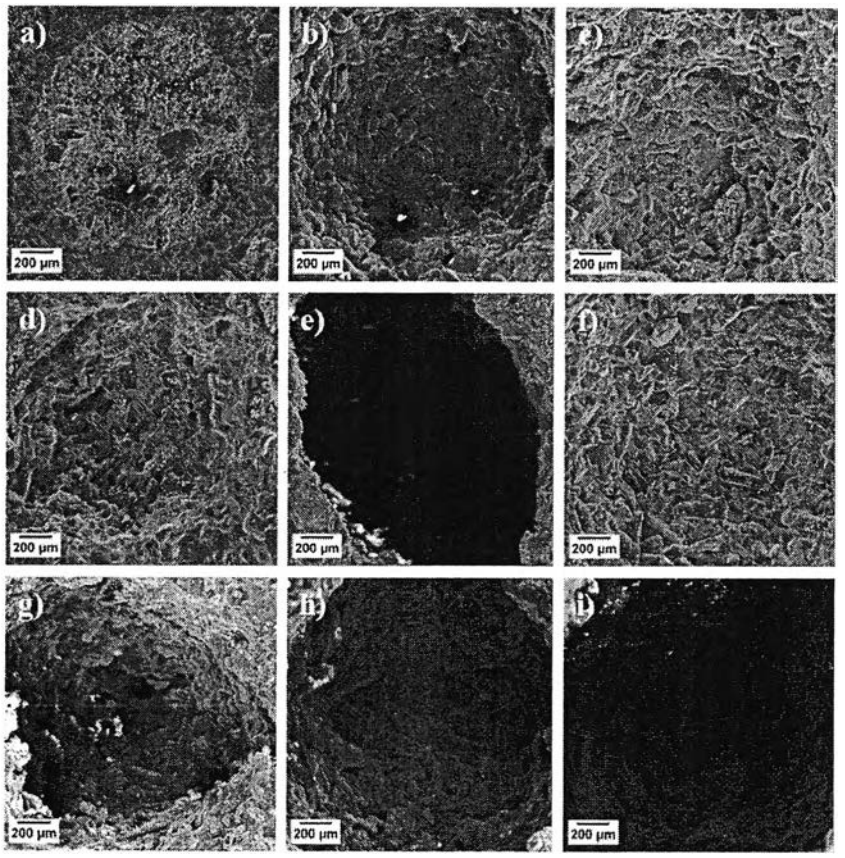

Figure 4.20 Surface of l-aspartic acid pellet at different flow rates at 20°C for 5 minutes (a) Before the experiment b) 40 ml/min c) 60 ml/min d) 80 ml/min e) 100 ml/min f) 120 ml/min g) 140 ml/min h) 160 ml/min i) 180 ml/min).

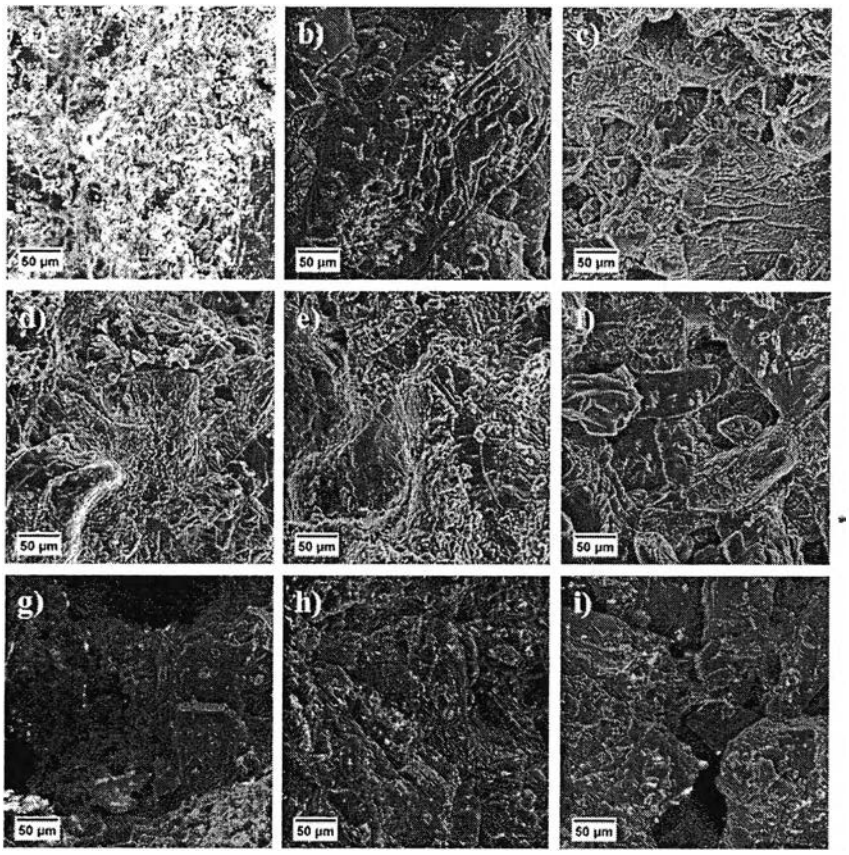

Figure 4.21 Surface of l-aspartic acid pellet at different flow rates at 20°C for 5 minutes (a) Before the experiment b) 40 ml/min c) 60 ml/min d) 80 ml/min e) 100 ml/min f) 120 ml/min g) 140 ml/min h) 160 ml/min i) 180 ml/min).

4.4.2 Weight Loss

Weight loss increase with flow rate is highly scattered. This suggests that another mechanism comes into play at higher flows – again, probably the increasing influence of particle release.

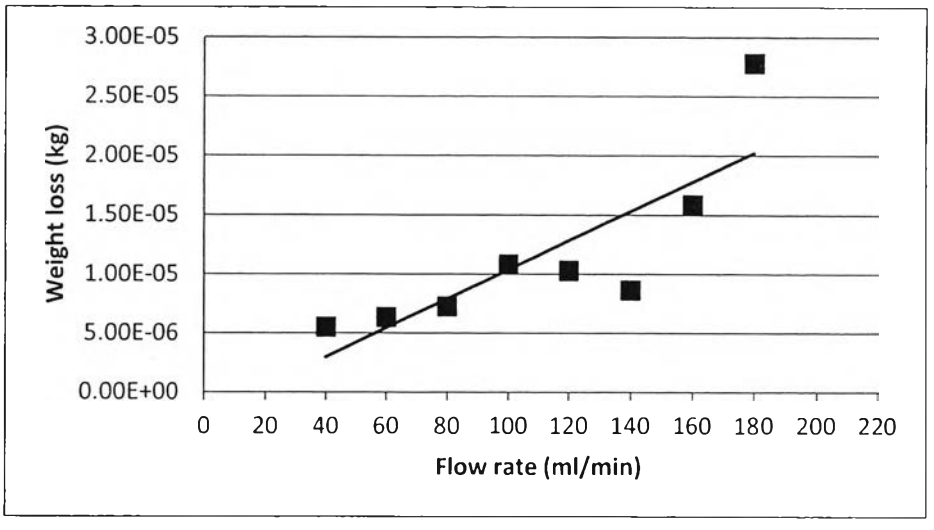

Figure 4.22 The effect of flow rate on weight loss of l-aspartic acid pellet.

Table 4.10 The effect of flow rate on volume lost and weight loss in L-aspartic acid

Flow rate ml/min	Volume m^3	Weight loss kg
180	2.18E-08	2.78E-05
160	1.24E-08	1.58E-05
140	6.77E-09	8.65E-06
120	8.06E-09	1.03E-05
100	8.48E-09	1.08E-05
80	5.69E-09	7.26E-06
60	4.97E-09	6.35E-06
40	4.32E-09	5.52E-06

4.4.3 Dissolution Rate

The dissolution rates of l-aspartic acid have the same trend with the weight loss. These phenomena can be explained by the non-uniform releasing of particles of l-aspartic acid.

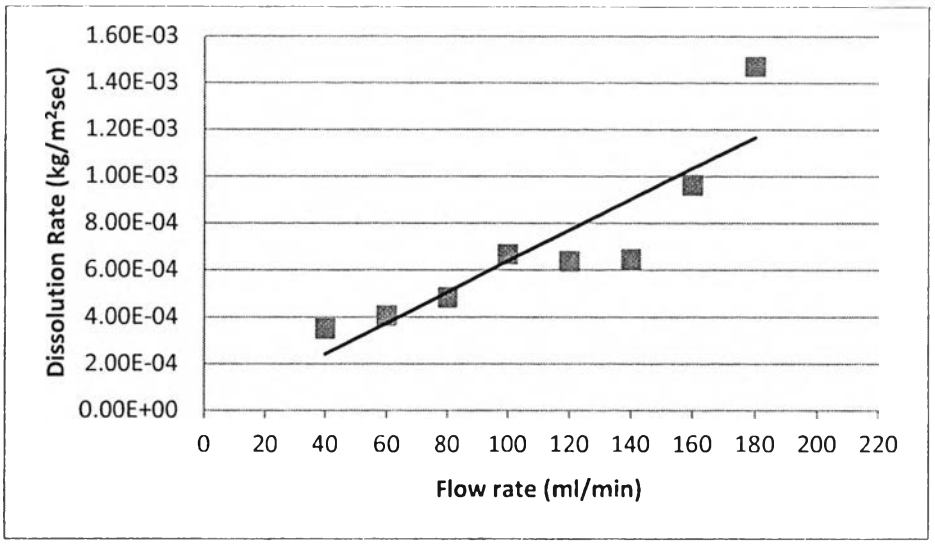

Figure 4.23 Dissolution rate of l-aspartic acid with different flow rates.

Table 4.11 Dissolution rate of l-aspartic acid with different flow rates

Flow rate ml/min	Dissolution Rate $kg/m^2 \times sec$
180	1.47E-03
160	9.62E-04
140	6.45E-04
120	6.37E-04
100	6.67E-04
80	4.83E-04
60	4.06E-04
40	3.51E-04

4.4.4 Overall Rate Constant

The overall rate constant of l-aspartic acid plot can be used to determine the dissolution rate constant. The average dissolution rate at 100, 120 and 140 ml/min is 1.33 m/s. This value correspond to the study of Shan et al. (2001) which determine from simulation of the change in crystal size distribution

(CSD) as 1.22 m/s at same temperature. However, the marked increase of overall rate constant can be explained by the releasing particles of aspartic acid.

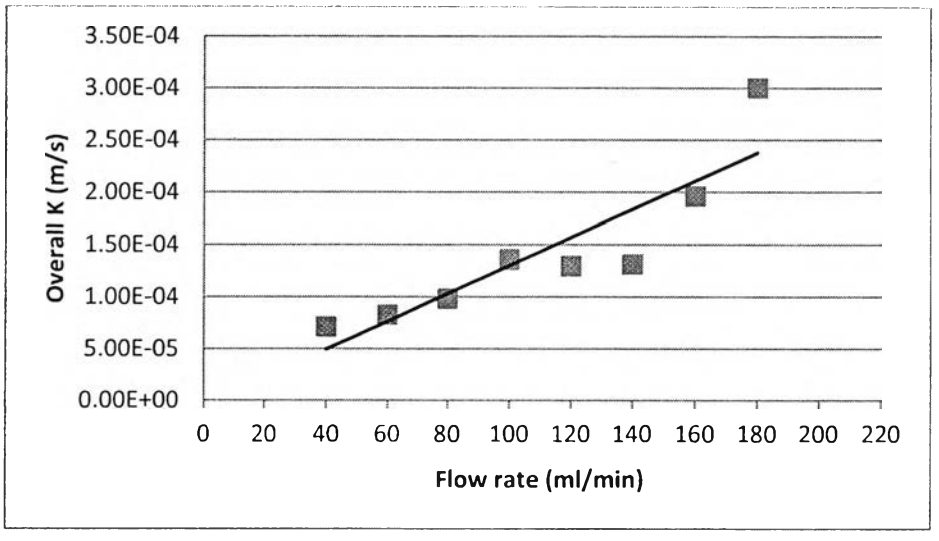

Figure 4.24 Overall rate constant of l-aspartic acid with different flow rates.

Table 4.12 Overall rate constant of l-aspartic acid with different flow rates

Flow rate ml/min	Overall K m/s
180	3.00E-04
160	1.96E-04
140	1.32E-04
120	1.30E-04
100	1.36E-04
80	9.85E-05
60	8.29E-05
40	7.15E-05

4.5 Trans-Cinnamic Acid

4.5.1 Pellet Surface Characteristics

Trans-cinnamic acid experiments were performed at 20 °C for 10 minutes at flow rates ranging from 40 to 180 ml/min. Craters in the pellet surfaces were difficult to see with naked the eye and also with the microscope (Figure 4.25). The surfaces before the experiments had scratch lines from polishing with sand paper. Dissolution was apparently non-uniform.

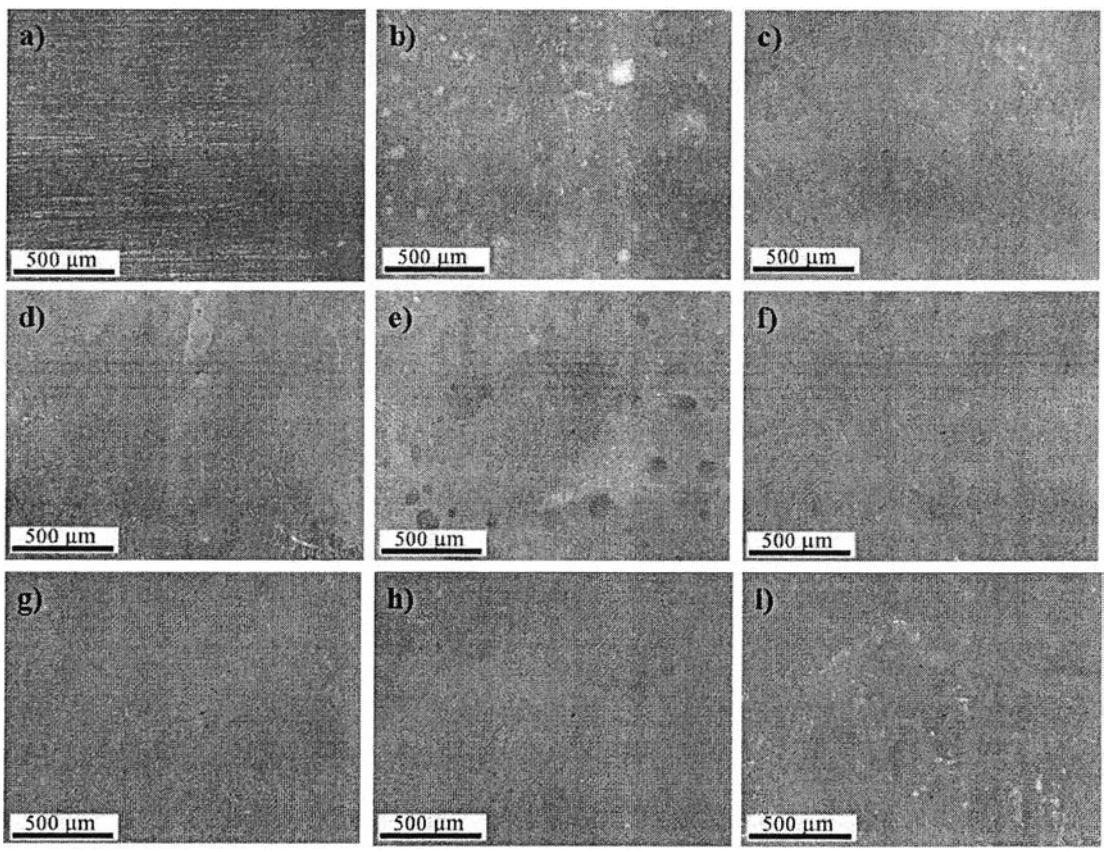

Figure 4.25 Surface of trans-cinnamic acid pellet at different flow rates at 20°C for 10 minutes (a) Before the experiment b) 40 ml/min c) 60 ml/min d) 80 ml/min e) 100 ml/min f) 120 ml/min g) 140 ml/min h) 160 ml/min i) 180 ml/min).

Figure 4.26 indicates that the impinging jet created rough surface of exposed crystals.

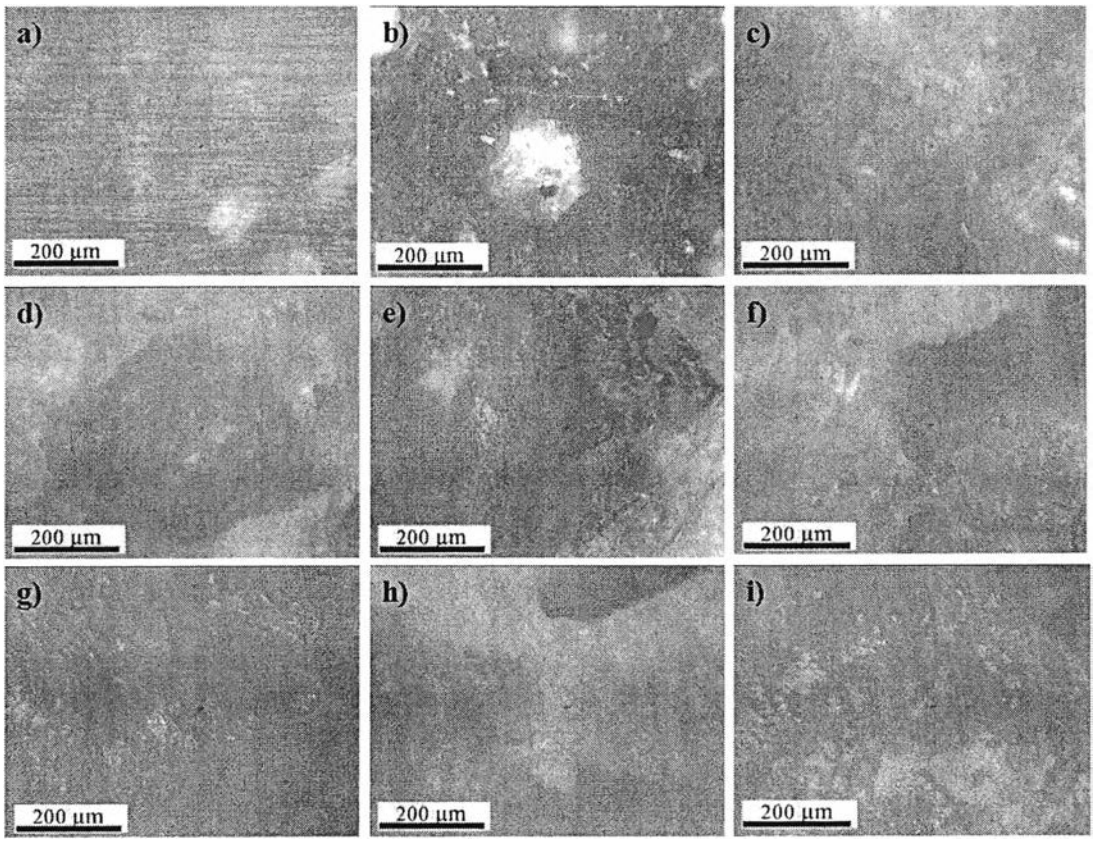

Figure 4.26 Surface of trans-cinnamic acid pellet at different flow rates at 20°C for 10 minutes (a) Before the experiment b) 40 ml/min c) 60 ml/min d) 80 ml/min e) 100 ml/min f) 120 ml/min g) 140 ml/min h) 160 ml/min i) 180 ml/min).

4.5.2 Weight Loss

Figure 4.27 indicates that the weight loss increase with flow rate is highly scattered.

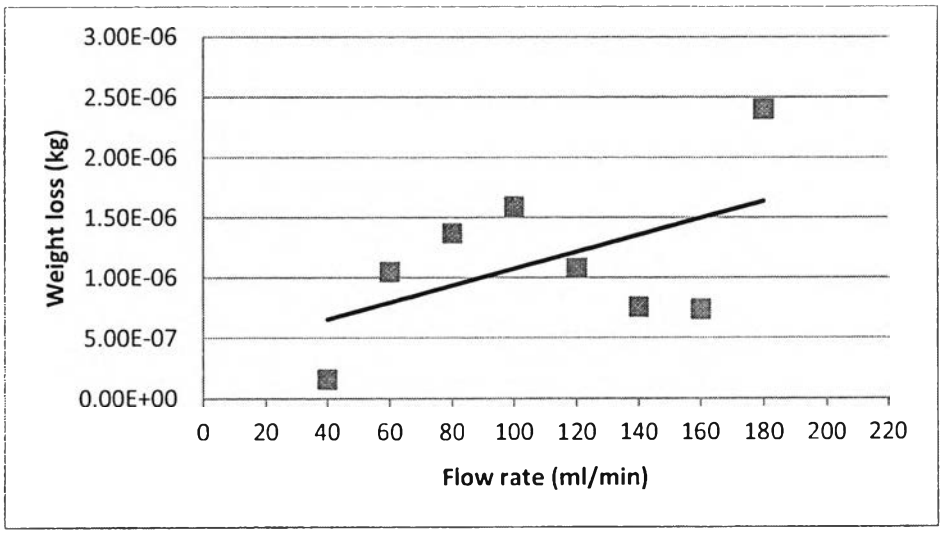

Figure 4.27 The effect of flow rate on weight loss of trans-cinnamic acid pellet.

Table 4.13 The effect of flow rate on volume lost and weight loss in trans-cinnamic acid

Flow rate ml/min	Volume m^3	Weight loss kg
180	1.30E-09	2.40E-06
160	4.01E-10	7.39E-07
140	4.11E-10	7.57E-07
120	5.86E-10	1.08E-06
100	8.65E-10	1.59E-06
80	7.44E-10	1.37E-06
60	5.69E-10	1.05E-06
40	8.69E-11	1.60E-07

4.5.3 Dissolution Rate

The dissolution rates of trans-cinnamic acid have the same trend with the weight loss. However, the plot of dissolution rate can explain that there is not the dissolution rate control in the system, since the dissolution rates are not leveling-off.

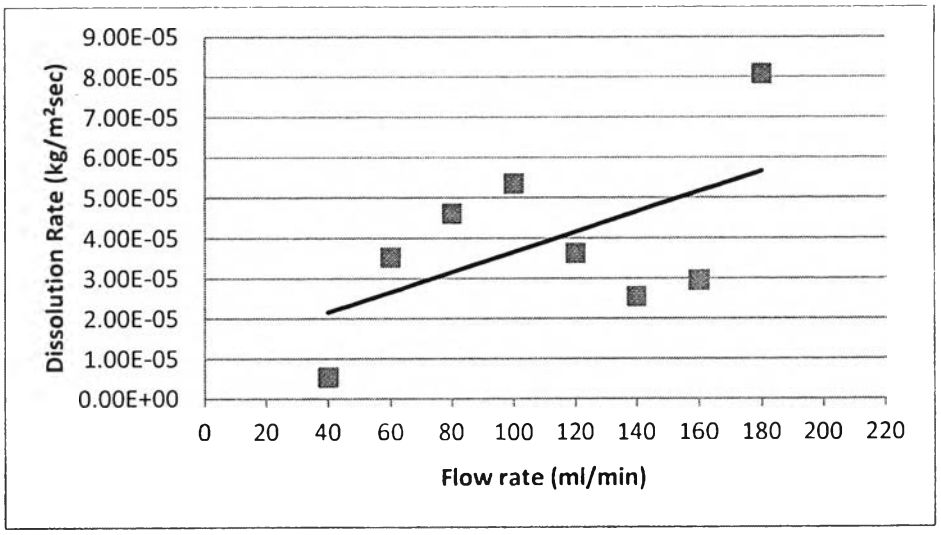

Figure 4.28 Dissolution rate of trans-cinnamic acid with different flow rates.

Table 4.14 Dissolution rate of trans-cinnamic acid with different flow rates

Flow rate ml/min	Dissolution Rate $kg/m^2 \times sec$
180	8.08E-05
160	2.96E-05
140	2.55E-05
120	3.63E-05
100	5.36E-05
80	4.61E-05
60	3.53E-05
40	5.39E-06

4.5.4 Overall Rate Constant

The overall rates of trans-cinnamic acid are in the same range as potassium bitartrate and aspartic acid. This led to a preliminary correlation for mass transfer versus flow for the apparatus that will be discussed later.

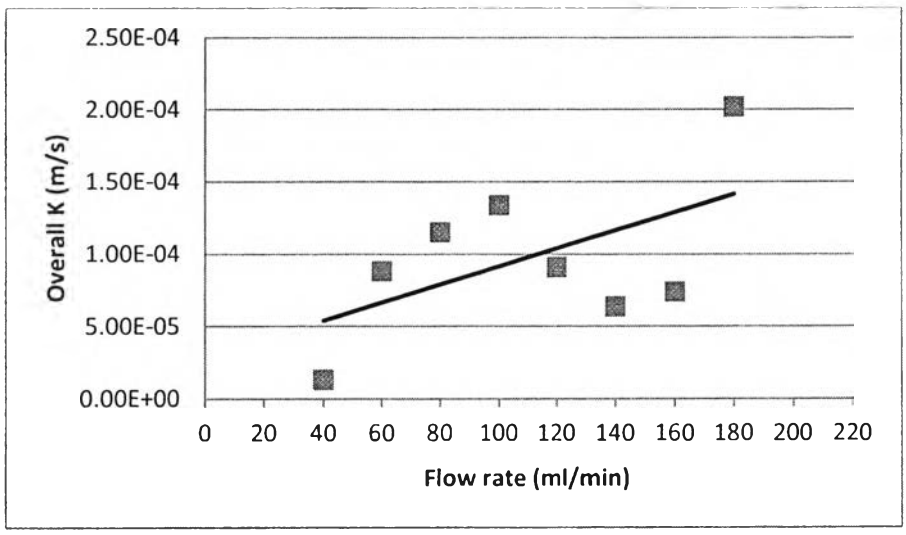

Figure 4.29 Overall rate constant of trans-cinnamic acid with different flow rates.

Table 4.15 Overall rate constant of trans-cinnamic acid with different flow rates

Flow rate ml/min	Overall K m/s
180	2.02E-04
160	7.39E-05
140	6.37E-05
120	9.09E-05
100	1.34E-04
80	1.15E-04
60	8.82E-05
40	1.35E-05

4.6 Single Crystal of Gypsum

4.6.1 Pellet Surface Characteristics

Changes in the surfaces of the single crystals were barely visible with the naked eye. Because the single crystals have less porosity than other material, the driving force of the jet cannot create a distinct crater in the crystal surface. For this

reason, the single crystals were exposed for longer times. Two sizes of single crystal were exposed at 120 ml/min for 30 minutes. Figure 4.30 shows the dissolution along the crystal because of the crystal structure. The direction of the scratches of the big crystal and the small crystal are the same. On the surface of the small crystal, there were crater lines along the crystal but on the surface of the big crystal, there were crater spots and some overlapped. These pits, related to the crystalline axes, are commonly referred to as being parallelogram-elongated (Chunfang, F. and Henry, T., 2007). This result suggests that the marks on the crystal surfaces were related to the crystal structure while scallops did not occur.

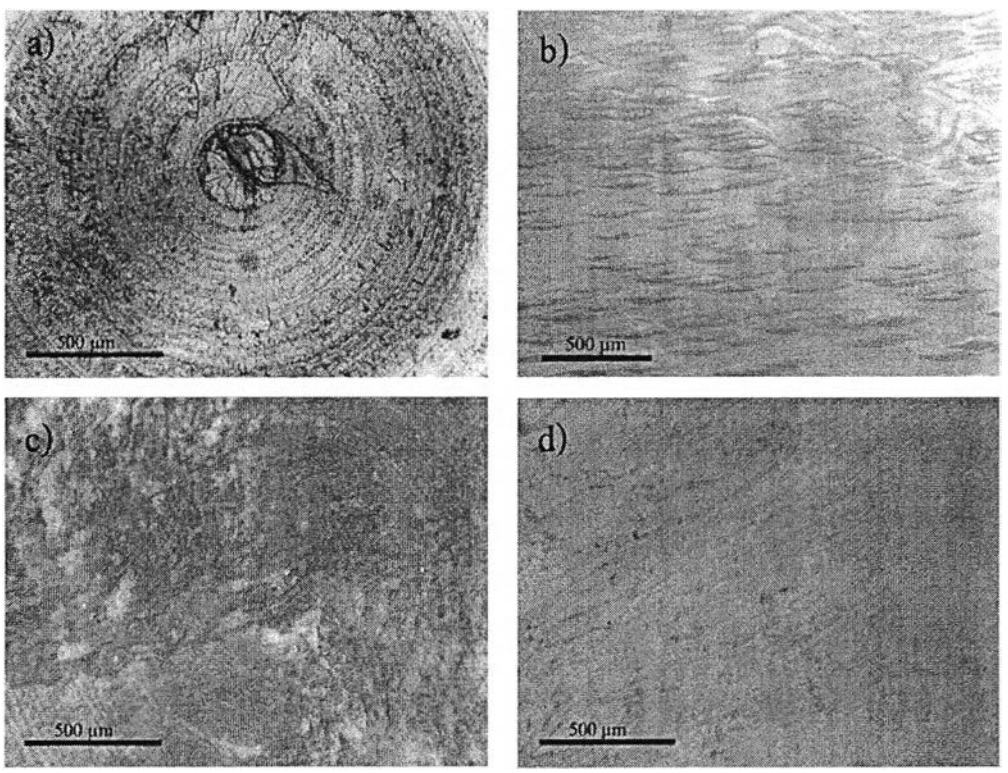

Figure 4.30 Surface of single crystals at different diameters exposed at 20°C for 30 minutes (a) big single crystal before experiment b) big crystal after the experiment c) small single crystal before experiment d) small single crystal after experiment).

4.6.2 Weight Loss

The weight loss of the big single crystal is slightly higher than that of the small crystal. These results are discussed later in terms of dissolution rate and the overall rate constant. In order to see the volume loss from the single crystal surfaces, profilometry was used to observe the roughness. In addition, the single crystals were marked to ensure that the same diameter was measured – before and after the experiment.

Table 4.16 The effect of pellet size on volume lost and weight loss in single crystal

Type	Volume m^3	Weight loss kg
Big Crystal	1.36E-10	3.15E-07
Small Crystal	1.30E-10	3.01E-07

4.6.3 Dissolution Rate

The dissolution rate estimated from weight loss of the big crystal was almost the same as the dissolution rate of the small crystal. It can be concluded that the dissolution rate of the single crystal is not dependent on dissolution area. Moreover, the comparison between the plaster and the single crystals showed that the dissolution rates of the single crystals (at flow rate of 120 ml/min) were lower than the dissolution rates of plaster at the lowest flow rate (40 ml/min). Because, the density of the plaster is lower than the density of the single crystal (about half) and the porosity is higher, diffusion through surface layers is easier and particles are readily released.

Table 4.17 Dissolution rate of single crystal with different size

Type	Dissolution Rate $kg/m^2 \times sec$
Big Crystal	7.08E-06
Small Crystal	6.75E-06

4.5.4 Overall Rate Constant

The overall rate constants between small and big single crystals are in good agreement. Moreover, the average value of the dissolution rate constant of the single crystal gypsum from the experiment (3.37E-06 m/s) is very close to published values of the dissolution rate constant of mineral gypsum at the same temperature (e.g., 3.36E-06 m/s from Colombani, J. and Bert, J., 2007). Since the dissolution rate constant of commercial plaster is greater than that of pure plaster (being at least 5.52E-04 m/s, Table 4.3), it is clearly that the form and purity of the studied material are important. These results provide some confidence in the experimental technique and reinforce the argument that results for the cast materials may be distorted by particle release.

Table 4.18 Overall rate constant of single crystal with different size

Type	Overall K m/s
Big Crystal	3.45E-06
Small Crystal	3.29E-06

4.7 Materials Comparison

4.7.1 Pellet Surface Characteristics

Inside the crater the porosity of each material is revealed. Figure 4.31 indicates that commercial plaster has large pores; they presumably affected the dissolution pattern. Pure plaster pores are smaller but their distribution is more regular. Potassium bitartrate porosity is low, no doubt because the powder was pressed at high pressure. On the other hand, aspartic acid (which was pressed at lower pressure) has large cracks inside the crater that appear to divide the solid into large particles. The trans-cinnamic acid pellet has surface cracks and a shallow crater. The gypsum single crystal surface has numerous shallow, aligned pits, some of which are commonly referred to parallelogram-elongated pattern.

These observations suggest that cast pellets may loosen and then release particles to different degrees as dissolution proceeds; at these higher flows, commercial plaster, pure plaster and aspartic acid apparently tend to release particles more that potassium bitartrate or trans-cinnamic acid. Single-crystal gypsum shows no tendency to release particles, only to dissolve more or less uniformly.

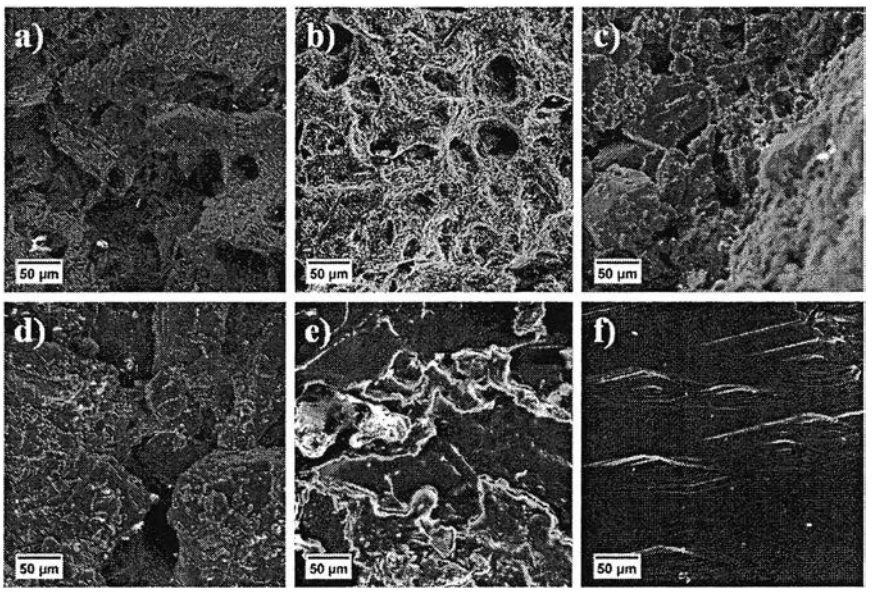

Figure 4.31 Surfaces of pellets of different materials (a) Commercial plaster at 199 ml/min b) Pure plaster at 180 ml/min c) Potassium bitartrate at 180 ml/min d) Aspartic acid at 180 ml/min e) Trans-cinnamic acid at 180 ml/min and f) Single crystal gypsum at 120 ml/min).

Figure 4.32 shows that the structure inside the commercial plaster and pure plaster are similar – both have needle-like crystals. The higher porosity of commercial plaster can be explained by Figure 4.33. The pure plaster structure is more packed than the commercial plaster with the smaller needle size, so the commercial plaster tends to release particles more than pure plaster. The structure of potassium bitartrate is also well-packed, presumably from formation at high pressure. However, small particles can be seen on the surface, suggesting that particles were released as dissolution proceeded. There are many large particles on the surface of l-aspartic acid, suggesting that the l-aspartic acid pellets easily release particles. Figure 4.33 at high magnification shows details of the cracks on trans-cinnamic acid and the parallelogram-elongated pattern of single crystal gypsum.

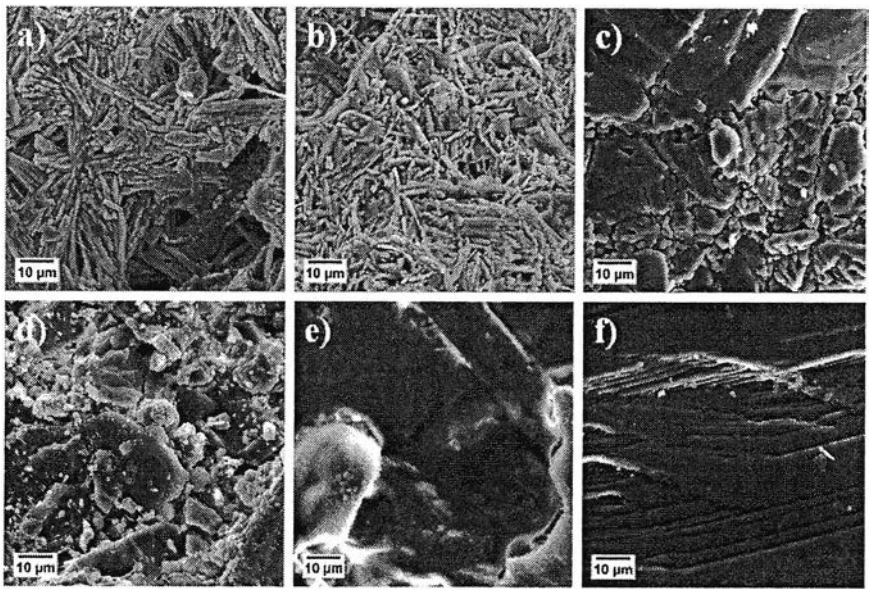

Figure 4.32 Surfaces of pellets of different materials (a) Commercial plaster at 199 ml/min b) Pure plaster at 180 ml/min c) Potassium bitartrate at 180 ml/min d) Aspartic acid at 180 ml/min e) Trans-cinnamic acid at 180 ml/min and f) Single crystal gypsum at 120 ml/min).

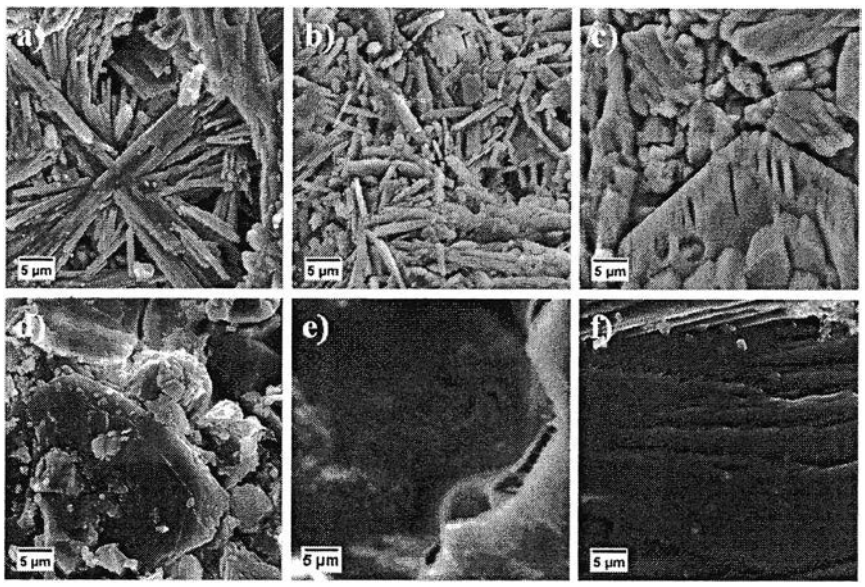

Figure 4.33 Surfaces of pellets of different materials (a) Commercial plaster at 199 ml/min b) Pure plaster at 180 ml/min c) Potassium bitartrate at 180 ml/min d) Aspartic acid at 180 ml/min e) Trans-cinnamic acid at 180 ml/min and f) Single crystal gypsum at 120 ml/min).

4.7.2 Weight Loss

From Figure 4.34, potassium bitartrate pellets are seen to have the highest weight loss, since potassium bitartrate has the highest solubility (6.17 g/l). The weight losses of commercial plaster and pure plaster are slightly different. At high flow rate the weight loss of pure plaster is clearly higher than commercial plaster because of the higher temperature of pure plaster. The overall weight loss of aspartic acid is lower than that of pure plaster; even though the solubility of l-aspartic acid (4.9 g/l) is higher than plaster (2.21 g/l). It can be deduced that the high porosity of plaster causes the higher weight loss. On the other hand, the weight losses of trans-cinnamic acid and single crystal are very close at the same flow rate (120 ml/min) and are lower than those of other materials, which supports the suggestion that crystals of gypsum and pellets of trans-cinnamic acid have higher density and lower porosity than other materials.

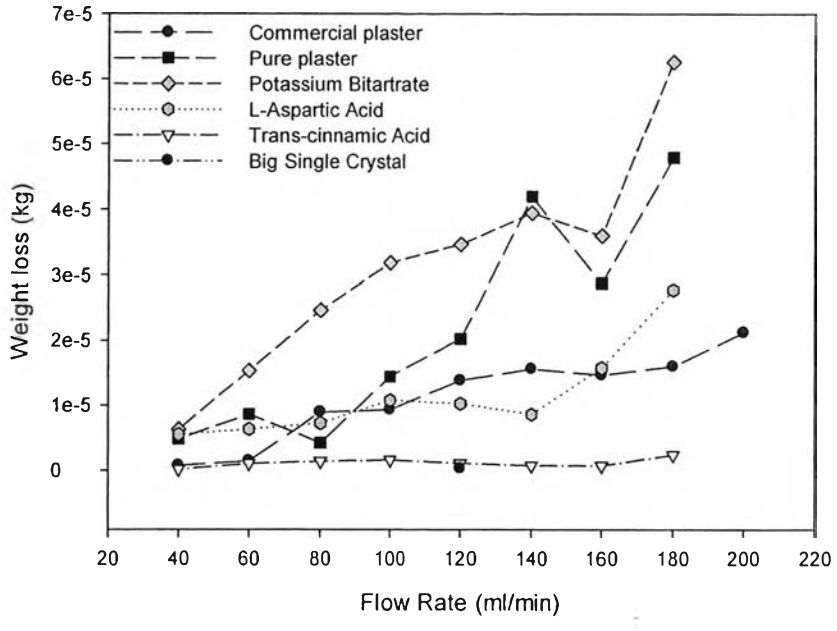

Figure 4.34 Weight losses of cast pellets of various materials.

4.7.3 Dissolution Rate

The highest dissolution rates are of commercial plaster; it has values tending to level-off at the highest flow rates (Figure 4.35). The dissolution rates of the other materials (at 20°C, except the pure plaster, which was at 34°C) are lower. The dissolution rate of l-aspartic acid, potassium bitartrate and pure plaster are in the same range. The trans-cinnamic acid and gypsum crystal are obviously lower than other material.

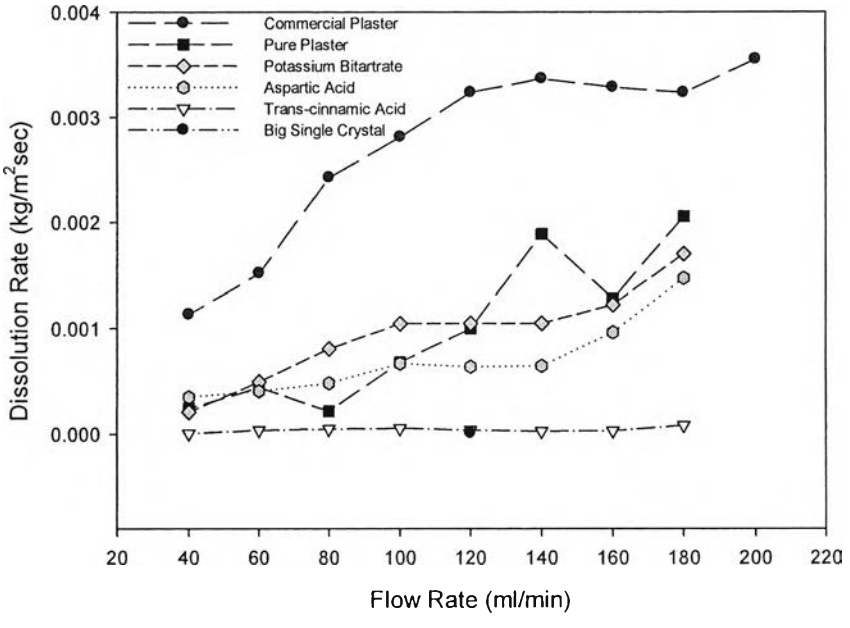

Figure 4.35 Dissolution rates of cast pellets of various materials.

4.7.4 Overall Rate Constant

The overall rate constant of commercial plaster is consistently higher than that of other materials. However, these results should be in the same range as those of other materials. It can be concluded that the effective solubility of commercial plaster is higher than that of pure plaster or single-crystal gypsum, even though the pure plaster was studied at a higher temperature. At the lowest flow rate, the overall rate constants of materials (except commercial plaster) are close to each other with an average value of 6.45E-05±5.10E-05m/s. This would be unusually low for a mass-transfer controlled process, so is likely to be influenced mostly by dissolution (discussed later) with any flow effects caused by particle or crystallite removal.

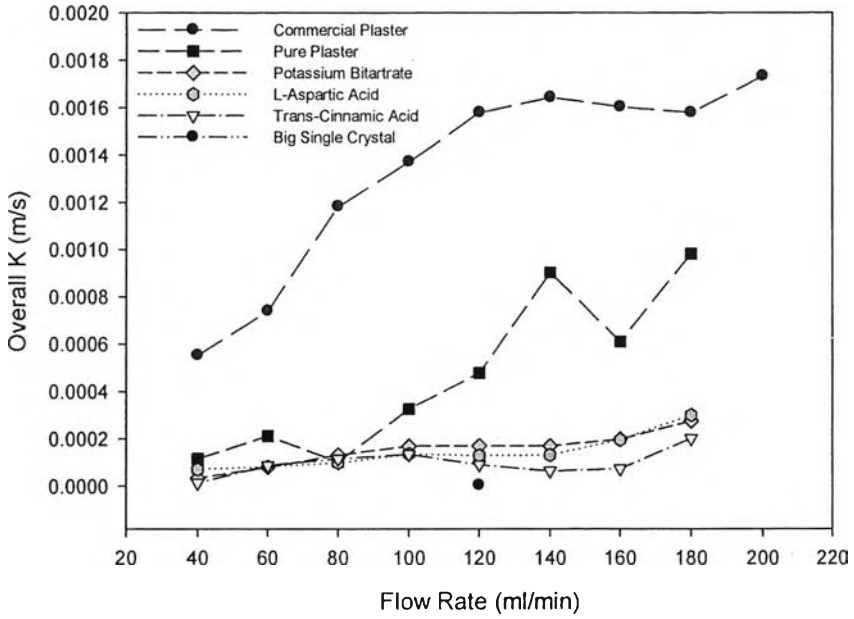

Figure 4.36 Overall rate constants of cast pellets of various materials.

4.8 Apparatus Correlations

As the experiments were carried out at different temperatures and with different materials, which affects the Schmidt number value, the log-log plots of Sherwood number divided by Schmidt number raised to the power 0.33 against Reynolds number for the liquid jet can lead to the apparatus correlation. The Schmidt number dependence in these correlations is obtained from published impinging-jet correlations; for example, the electrochemical study of jet impingement of Chin, D-T. and Tsang, C-H. 1978. Since Schmidt number determination would involve changing the parameters – notably, diffusivity and viscosity – which is achieved by changing temperature, a more precise power of Schmidt number would be obtained from further experiments conducted over a wider range of temperature.

Since the pure plaster is mixed control between dissolution and mass transfer and the potassium bitartrate dissolution constant is unknown, these two materials are not suitable to determine the apparatus correlation.

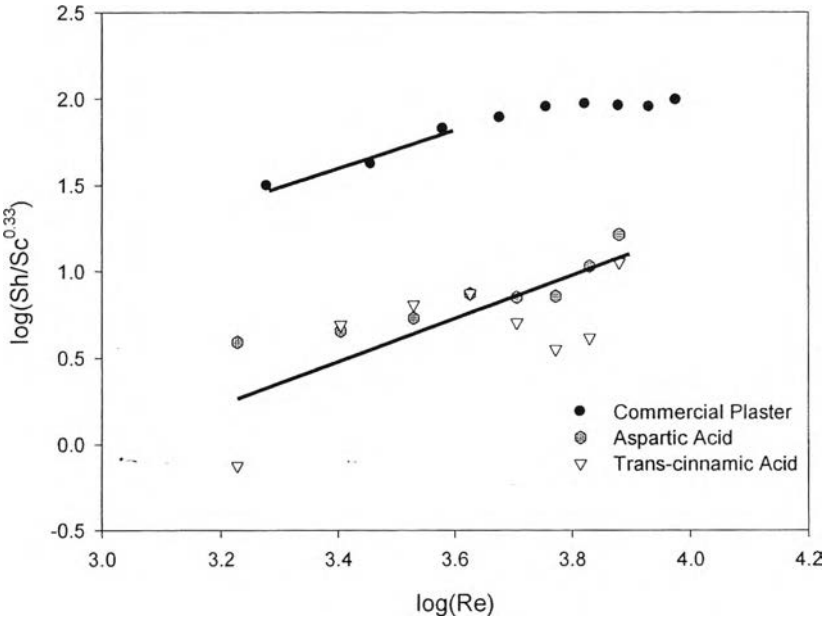

Figure 4.37 Sherwood number plots for dissolution of cast pellets of various materials.

In Figure 4.37, the plot shows that Sherwood numbers divided by Schmidt number for the aspartic acid and trans-cinnamic acid are in the same range. The correlation can be found as:

$$Sh = 2.29E\text{-}03\ Re^{0.94}Sc^{0.33} \tag{4.1}$$

On the other hand, the data at lower flows (where mass transfer rate is the limiting step) for the commercial plaster produces the correlation:

$$Sh = 9.05E\text{-}03Re^{1.07}Sc^{0.33} \tag{4.2}$$

Equations 4.1 and 4.2 can be compared with the correlations of Rao and Trass (1964) that is $Sh = 0.046Re^{1.06}(H/d_0)^{-0.09}$ and Chin and Tsange (1978) that is $Sh = 1.12Re^{0.5}(H/d_0)^{-0.057}$ because they were developed base on a submerged jet similar to the experimental apparatus used in this study in which H/d_0 is relative jet length. For this study of jet geometry, H is 3.0 mm and d_0 is 0.5 mm, the Schmidt number of

$CaSO_4.2H_2O$ at 25°C (983) and the average Schmidt number of aspartic acid and trans-cinnamic acid at 20°C (1122) can be used to transform experiment correlations. The Reynolds numbers at 180 ml/min and 20°C for aspartic acid and trans-cinnamic acid correlation and 80 ml/min and 25°C for commercial plaster correlation are also used to determine Sherwood number (Table 4.19).

Table 4.19 Comparison of Sherwood number from different correlations

Correlation	Re utilized for calculation	Sherwood number Comparison in different conditions		Re range (Minimum<Re< Maximum)
		Comerci-al plaster	Trans-cinnamic acid	
$Sh = 9.05E\text{-}03Re^{1.07}Sc^{0.33}$ (Commercial plaster)	3802	595	-	1900<Re<3802
$Sh = 2.29E\text{-}03\ Re^{0.94}Sc^{0.33}$ (Aspartic acid and Trans-cinnamic acid)	7610	-	103	1690<Re<7610
$Sh = 1.12Re^{0.5}(H/d_0)^{-0.057}$ (Chin&Tsange)	3802	606	-	4000<Re<16000
	7610	-	895	
$Sh = 0.046Re^{1.06}(H/d_0)^{-0.09}$ (Rao&Trass)	3802	244	-	20000<Re <125000
	7610	-	509	

The Sherwood number from the aspartic acid and trans-cinnamic acid correlations is much lower than published expressions for similar equipment, no doubt because of dissolution having the major effect.

On other hand, the Sherwood number from the commercial plaster correlation is closer to the Sherwood number from the Chin and Tsange correlation (percentage error = 2%) than to that from the Rao and Trass correlation (percentage

error = 59%). Deviations from the published expression are probably due to the ranges of Reynolds number in the literature (Chin and Tsange; 4000<Re<16000, Rao and Trass; 20000<Re<125000) that are higher than in this experiment (1910<Re<3802), as well as to the effects of particle release.